Terahertz time-domain measurement of ballistic electron resonance in a single-walled carbon nanotube

ZHAOHUI ZHONG[1], NATHANIEL M. GABOR[1,2], JAY E. SHARPING[3†], ALEXANDER L. GAETA[1,3] AND PAUL L. McEUEN[1,2*]

[1]Center for Nanoscale Systems, Cornell University, Ithaca, New York 14853, USA
[2]Laboratory of Atomic and Solid-State Physics, Cornell University, Ithaca, New York 14853, USA
[3]School of Applied and Engineering Physics, Cornell University, Ithaca, New York 14853, USA
[†]Present address: School of Natural Sciences, University of California at Merced, Merced, California 95344, USA
*e-mail: mceuen@ccmr.cornell.edu

Published online: 23 March 2008; doi:10.1038/nnano.2008.60

Understanding the physics of low-dimensional systems and the operation of next-generation electronics will depend on our ability to measure the electrical properties of nanomaterials at terahertz frequencies (~100 GHz to 10 THz). Single-walled carbon nanotubes are prototypical one-dimensional nanomaterials because of their unique band structure[1,2] and long carrier mean free path[3–5]. Although nanotube transistors have been studied at microwave frequencies (100 MHz to 50 GHz)[6–11], no techniques currently exist to probe their terahertz response[12]. Here, we describe the first terahertz electrical measurements of single-walled carbon nanotube transistors performed in the time domain. We observe a ballistic electron resonance that corresponds to the round-trip transit of an electron along the nanotube with a picosecond-scale period. The electron velocity is found to be constant and equal to the Fermi velocity, showing that the high-frequency electron response is dominated by single-particle excitations rather than collective plasmon modes. These results demonstrate a powerful new tool for directly probing picosecond electron motion in nanostructures.

Electromagnetic signals in the terahertz (THz) frequency range are important both for fundamental materials research and for technical applications in security, biological sensing/imaging and high-speed communications[13,14]. The size and resolution of THz devices based on electromagnetic waves are invariably hundreds of micrometres, set by the wavelength of the radiation. Nevertheless, there is great potential for a synergy between THz technology and another rapidly growing area of research, nanoscience and nanotechnology. The reason for this is that electrons in solids travel hundreds of times slower than light, and therefore electron dynamics in micro- and nanostructures typically fall in the THz frequency region. This not only creates opportunities to use existing THz technologies to study electron propagation in these structures, but also opens up the possibility that ballistic nanodevices could be used to create new kinds of THz sources or detectors[15].

Single-walled carbon nanotubes are an excellent candidate for THz electron dynamics experiments. Electrical measurements have demonstrated ballistic electron motion over micrometre scales[3–5], suggesting a fast electron transit on the picosecond timescale. From Tomonaga–Luttinger theory of one-dimensional electron gases, two kinds of high-frequency excitations in nanotubes are predicted: single-particle excitations that move at the Fermi velocity v_F (determined by band structure), and collective or plasmon excitations that propagate at the plasmon velocity $v_{pl} = v_F/g$ ($0 < g < 1$, set by both the band structure and the electronic environment of the nanotube)[16,17]. Previous d.c. transport measurements revealed an interference pattern consistent with electrons propagating at the Fermi velocity[18,19]. However, it is currently not known whether the single-particle excitations or the plasmon excitations will dominate the high-frequency response of a nanotube[20,21]. This question can be answered by a direct time-domain measurement of electron transit time.

In this work, we perform THz electrical measurements on single nanotubes. By integrating a THz source and a carbon nanotube transistor on the same substrate, high-frequency signals are generated locally by the source and detected locally by the nanotube transistor. Using this technique, we directly probe the electron motion in the time domain along the tube, finding a prominent resonance corresponding to ballistic propagation of the electrons through the device. The speed of this dominant excitation is found to be given by the Fermi velocity and not the plasmon velocity.

Figure 1a shows a schematic of a single-walled carbon nanotube field-effect transistor integrated with the THz source. We fabricated the transistor with both a metal topgate and global silicon backgate on a silicon-on-sapphire (SOS) substrate (see Methods), as shown on the left-hand side of the schematic. We then chose devices containing only one quasi-metallic single-walled carbon nanotube, that is, a nanotube with small bandgap E_g of tens of meV due to curvature or strain, as determined by atomic force microscopy (AFM) and d.c. transport studies[22–24] (see Supplementary Information, Fig. S1). The THz source[25,26] consists of a microwave transmission line, fabricated directly on the silicon layer, that is excited by a short-pulse laser, as

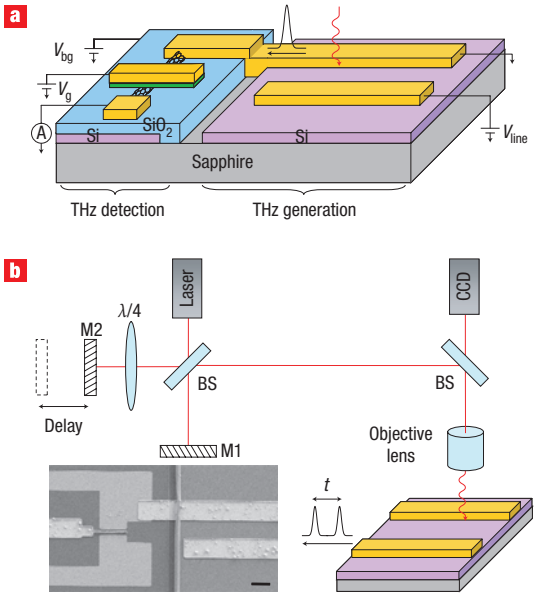

Figure 1 Device geometry and measurement setup for THz electrical transport study of a single-walled carbon nanotube. a, Device schematic showing the THz source integrated with a nanotube transistor. The metal electrodes are shown in gold, the SiO topgate dielectric in green, SiO_2 in blue, the silicon layer in pink, and the sapphire layer in grey. Femtosecond laser excitation (red wavy arrow) generates picosecond voltage pulses, which are then transmitted to the nanotube transistor. **b**, Schematic of two-pulse time delay autocorrelation measurement. The laser beam is split by the beamsplitter (BS) into two beams with equal intensity. The reference beam is reflected by a fixed mirror (M1), and the delay beam is reflected by a mirror (M2) mounted on a motorized translation stage to introduce a time delay. The $\lambda/4$ waveplate rotates the polarization of the delay beam by 90° with respect to the reference beam in order to avoid interference from the laser. These two beams are then recombined and focused down to the transmission line gap, generating two voltage pulses with controllable time delay t_D. The inset shows a scanning electron microscopy (SEM) image of a device. Scale bar, 10 μm. Only the transistors containing one quasi-metallic single-walled carbon nanotube are studied. Their chirality is not known.

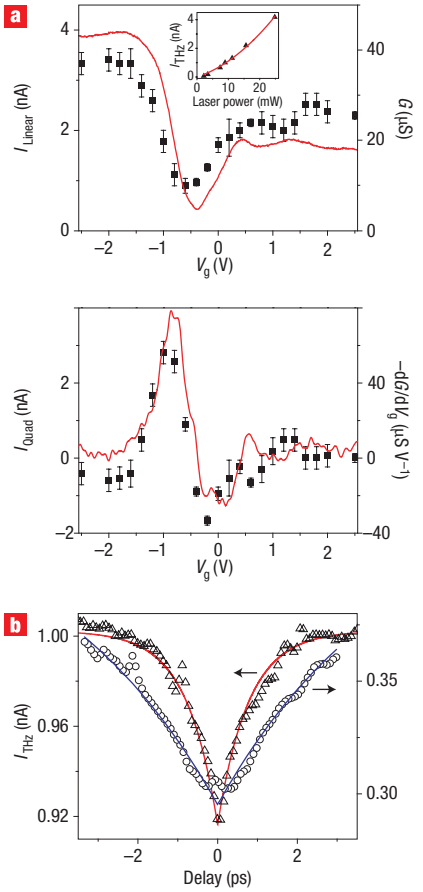

Figure 2 Single-walled carbon nanotube THz detector. a, Carbon nanotube THz responses with single laser beam excitation. The inset shows the I_{THz} versus laser power plot at $V_{line} = 50$ V and $V_g = -1$ V. The red curve is the fit with both linear (I_{linear}) and quadratic terms (I_{quad}), $I_{THz} = I_{linear}(P/P_0) + I_{quad}(P/P_0)^2$, where P/P_0 is the normalized laser power, and $P_0 = 24.8$ mW. I_{linear} obtained at various topgate voltages V_g is plotted as black squares in the top panel. I_{quad} obtained at various topgate voltages V_g is plotted as black squares in the bottom panel. G and $-dG/dV_g$ are also plotted as the red curves in the top and bottom panels, respectively, for comparison. The picosecond voltage pulse amplitude can be estimated from $V_{THz} = I_{linear}/(Gwf)$, where w and f are the voltage pulsewidth and the repetition rate of the laser, respectively. Other sources of nonlinearity in the $I-V$ curves, such as metal-nanotube Schottky contacts and current saturation (see Supplementary Information, Fig. S1), are also present in our measurement, such as the finite I_{quad} obtained around $V_g = -2.5$ V, where dG/dV_g is small. **b**, Two-pulse time delay measurement. Open triangles are I_{THz} measured at $V_g = 2.5$ V (left axis), and open circles are I_{THz} measured at $V_g = -0.3$ V (right axis). The red and blue curves are the fits with exponential decay, $I_{THz} = A + Be^{-|t|/\tau}$.

shown on the right-hand side of the schematic. The ground line of the transmission line was connected to the drain electrode of the nanotube transistor. The THz signal was generated by biasing the transmission line with a d.c. voltage V_{line} and photo-exciting the transmission line gap with a femtosecond Ti:sapphire laser (see Methods). Each ultrashort laser pulse produces a unipolar voltage pulse with a pulsewidth of 1–1.5 ps, corresponding to a broadband THz signal. The amplitude of the voltage pulse V_{THz} scales linearly with laser power P and V_{line} (see Supplementary Information, Fig. S2). The fast voltage pulse is transmitted along the transmission line to the nanotube transistor, applying a voltage pulse across the nanotube device. We then recorded the d.c. current response to the THz pulses, I_{THz}. To access the time domain, each laser pulse was split into two before illuminating the transmission line gap, resulting in two picosecond voltage pulses with controllable delay time t_D (Fig. 1b). Measuring I_{THz} as a function of the delay time yields information on the device response at picosecond timescales.

We first measured the THz $I-V$ characteristics of these nanotube devices. The inset to Fig. 2a shows I_{THz} as a function of laser power at a topgate voltage $V_g = -1$ V, taken on the device with a topgate length $L_g = 3.2$ μm at 150 K. We found that the current has both linear, I_{linear}, and quadratic, I_{quad}, dependence on the laser power and hence the voltage pulse amplitude. We plotted I_{linear} and I_{quad} for various V_g and compared I_{linear} with the d.c. conductance (G), and I_{quad} with negative transconductance ($-dG/dV_g$), in the top and bottom panels of Fig. 2a, respectively. We see clearly that I_{linear} follows the gate-dependent conductance curve, and I_{quad} follows the gate-dependent transconductance curve. The correlation between $I_{THz}-V_{THz}$ and d.c. transport characteristics indicates that the

nanotube transistor functions similarly at both d.c. and THz frequencies:

$$I = GV - \frac{1}{2}\frac{dG}{dV_g}V^2,$$

where the current contains a linear term proportional to the conductance and a quadratic term proportional to the transconductance[9]. From I_{linear} and G we obtain an estimate of the picosecond voltage pulse amplitude; amplitudes V_{THz} of $\sim$0.1–0.25 V are typical. A similar estimate of V_{THz} can be obtained from I_{quad} and dG/dV_g with comparable results. This demonstrates that the response of the device (both linear and nonlinear) is similar at d.c. and THz frequencies, and further that the nonlinear THz response is dominated by the gating action of the transistor.

We now explicitly measure the response speed of the carbon nanotube device through the two-pulse time delay measurement. Figure 2b shows I_{THz} as a function of delay time. The open triangles are data taken at $V_g = 2.5$ V, where the device has a resistance of 55 kΩ, and the open circles are data taken at $V_g = -0.3$ V, where the device has a resistance of 180 kΩ. In both curves, I_{THz} shows a clear inverse peak centred at a delay time $t_D = 0$ when the two pulses overlap. This peak is caused by the nonlinear response of the device. Two overlapping pulses generate a larger nonlinear term than the same two pulses separated by the response time of the device. Fitting these curves with an exponential decay yields the device response time τ. It increases from 0.9 ps to 2.5 ps as the resistance of the device increases from 55 kΩ to 180 kΩ. This picosecond-scale device response time proves that the nanotube transistor functions as a fast THz detector.

We can use the fast response time to probe ballistic electron transport through the nanotube in the time domain. Figure 3 shows the two-pulse time delay measurements on three quasi-metallic single-walled carbon nanotubes with topgate lengths L_g of 1.5 μm (black), 3.2 μm (red) and 4.9 μm (green). The nanotubes are gated in a p–n–p configuration, by electrostatic n-doping the section underneath the topgate while maintaining the rest of the nanotube p-doped by the backgate (Fig. 3a). For all three devices (Fig. 3b), the I_{THz} versus delay time t_D shows an inverse peak at $t_D = 0$ and at least one set of satellite peaks symmetrically located around the central peak. For the device with $L_g = 1.5$ μm, we observe a single set of satellite peaks at $t_D = \pm 4.4$ ps. For devices with $L_g = 3.2$ and 4.9 μm, we clearly observe two sets of satellite peaks with repetition period $t_r \approx 8$ and 11.5 ps, respectively.

We interpret these peaks as a ballistic electron resonance in the single-walled carbon nanotube cavity bounded by p–n junctions. The electrons excited by the first THz pulse traverse the first p–n junction, propagate along the length of the nanotube, and are reflected at the second p–n junction. At $t = t_r$, the returning electrons meet the incoming electrons excited by the time-delayed pulse. Larger nonlinear current is generated in the same manner as at $t = 0$, resulting in the satellite peaks in Fig. 3b. The observed period t_r therefore corresponds to the round-trip transit time of an electron within the nanotube cavity. The observation of a second peak at $2t_r$ in the longest device ($L = 4.9$ μm) indicates that electrons can travel ballistically up to $4L \approx 20$ μm within the nanotube cavity. This finding is consistent with the long mean free path of $\sim$10 μm observed in quasi-metallic nanotubes at $T = 100$ K (ref. 5). Our result represents the first direct time-domain measurement of electron transit in a carbon nanotube. For the longer two devices, we also notice peak splitting for the first resonance (most noticeable in the green curve), the nature of which is not understood.

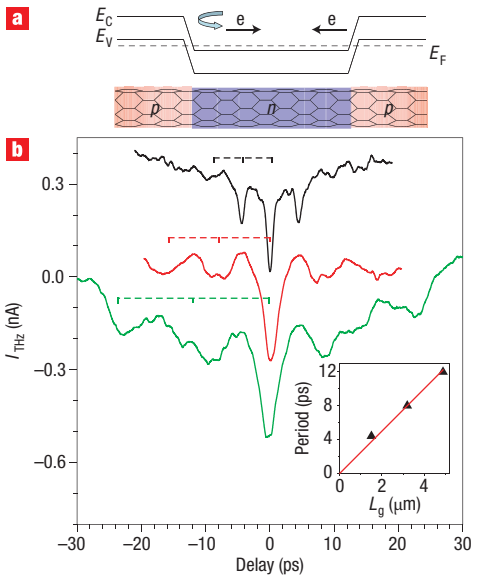

Figure 3 Time-domain direct detection of ballistic electron resonance. **a**, Schematic of the resonance cavity formed by differential gating along the carbon nanotube. The nanotube section underneath the topgate electrode is electrostatic doped n-type (blue), and the rest of the nanotube is doped p-type (red), forming two p–n junctions. **b**, Ballistic electron resonance measured for three devices with different gate lengths, $L_g = 1.5$ μm (black), 3.2 μm (red) and 4.9 μm (green). The measurement temperature was 150 K for the black and red curves and 100 K for the green curve. The data were taken at estimated voltage pulse intensities of $V_{THz} \approx 0.25$ V, 0.25 V and 0.3 V for the devices with $L_g = 1.5$ μm, 3.2 μm and 4.9 μm, respectively. For each pulse, 10–100 electrons were collected, as determined from $N = I_{THz}/(fe)$. For ease of comparison, the curves are offset, and the red curve is multiplied by 3 and the black curve by 2. Dotted colour lines mark out the resonance period $t_D = t_r$ and $t_D = 2t_r$. The inset shows the resonance periods versus device topgate lengths (black triangles) with a linear fit (red).

To determine the velocity of the excitation, we plotted t_r for three devices versus their topgate lengths (Fig. 3b inset). The linear fit of t_r versus L_g yields an electron velocity $v = 2L_g/t_r \approx 0.8 \pm 0.1 \times 10^6$ m s^{-1}. This is in good agreement with the Fermi velocity of electrons in metallic carbon nanotubes, 0.8×10^6 m s^{-1}, but significantly less than that expected for the plasmon mode ($v_{pl} = 2.7 \times 10^6$ m s^{-1} for $g = 0.3$)[27]. This demonstrates that single-particle excitations, not the plasmon mode, dominate the high-frequency response in our measurement.

The dominance of single-particle excitations may result from the fourfold degeneracy of the nanotube's one-dimensional subband[1]: two from the spin degeneracy and two from the sublattice degeneracy. Three of the degenerate modes are single-particle-like neutral modes that propagate at v_F; only a single (faster) plasmon mode propagates at v_{pl} (refs 16,17). Assuming that each mode has the same probability of being excited by the THz pulse, the neutral modes will provide the dominant response, but further theoretical work is needed in order to substantiate this conjecture. The plasmon mode is not seen in our current experiments, but it may be observable with higher time resolution and improved signal-to-noise ratio.

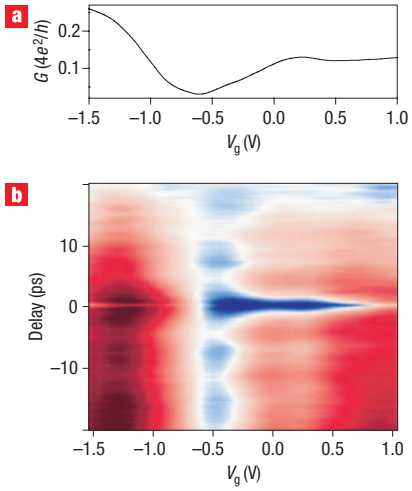

Figure 4 Gate-voltage dependence of the electron resonance. **a**, The conductance versus gate voltage. **b**, Current versus V_g and delay time is plotted in a two-dimensional colour scale. Data were taken for the device with $L_g = 3.2\ \mu m$, at $V_{THz} \approx 0.25$ V, and the measurement temperature was 150 K. Baseline currents are subtracted for the ease of comparison, and current value ranges from −0.15 nA (dark blue) to 0.32 nA (dark red). The disappearance of resonance at gate voltages away from the gap region ($V_g < -1.3$ V or $V_g > 0.7$ V) may be caused by enhanced electron tunnelling through the p–n junctions or by the diminished nonlinear signal as dG/dV_g approaches zero.

To examine the dependence of the velocity on the electron density, we plot in Fig. 4 the two-dimensional map of I_{THz} (in colour scale) versus the delay time and the topgate voltage for the device with $L_g = 3.2\ \mu m$. The d.c. conductance versus V_g curve is also shown. The resonance is most pronounced when the nanotube section underneath the topgate is n-doped at $V_g \approx -0.4$ V and is reproducible over a range of topgate voltages, from $V_g \approx -1.3$ V to 0.7 V. No resonance is observed at $V_g < -1.3$ V or $V_g > 0.7$ V. Over the observable range, the positions of the ballistic resonance peaks do not shift with topgate voltage, indicating that the propagation velocity does not depend on the electron density in the nanotube. Similar behaviour was seen for all devices examined.

The density-independent velocity follows from the unique band structure of metallic carbon nanotubes: a linear dispersion relationship yields a constant Fermi velocity independent of Fermi energy[1]. This constant velocity makes quasi-metallic nanotubes uniquely suited for the observation of ballistic electron resonance. Although a small bandgap exists in a quasi-metallic nanotube, large excitation voltages, $V_{THz} \gg E_g$, mean that most electrons have energy into the linear region. A single resonance period occurs because the majority of electrons travel at the same velocity. These properties make carbon nanotubes excellent candidates for use as compact THz resonators. Because electrons in nanotubes travel hundreds of times slower than light, nanotube ballistic THz resonators are micrometre scale instead of ∼300 μm. Furthermore, nanotube transistors possess intrinsic gain that, when combined with their potential as resonators, may create possible new classes of miniaturized THz sources.

The measurement technique developed in this work is a powerful new tool for directly measuring THz dynamics in individual nanoscale structures. It opens the door to time-domain electrical measurements of many other systems, such as graphene[28] and semiconductor nanowires[29]. It should find broad application in exploring the electrical, magnetic and electromechanical excitations of nanoscale devices.

METHODS

DEVICE FABRICATION

The devices were fabricated on the intrinsic silicon-on-sapphire substrate with 150-nm SiO_2. Carbon nanotubes were grown from predefined Fe-Mo catalysts using the chemical vapour deposition (CVD) method and contacted by 35-nm Pd as the source and drain electrodes. The top metal gates (with 15-nm thermal evaporated SiO as dielectric) were separated from source and drain electrodes by 500 nm in order to minimize parasitic capacitance. Transmission line structures (3 mm long), consisting of two 15-μm-wide Ti/Au (10/300 nm) lines separated by 5 or 10 μm, were deposited directly onto the intrinsic silicon layer of the SOS substrate (with the SiO_2 layer etched away). At the end of fabrication, the i-Si on the THz generation side was heavily damaged by O^+ ion implantation[26], and the nanotube transistors' part was protected by photoresist film as a mask.

THz generation and detection

For THz generation, a femtosecond Ti:sapphire laser centred at 813 nm (<200 fs pulsewidth, 75 MHz repetition rate) was used to photo-excite the transmission line gap at a distance of ∼150 μm away from the nanotube, and the transmission line biased with V_{line} (ref. 26). The d.c. current passing through the nanotube transistor was measured with both its source and drain electrodes grounded, in order to make sure that the current was purely a result of the nanotube responses to the picosecond voltage pulses. During the measurement, the topgate voltage V_g was tuned from −3 V to 3 V, and the backgate voltage V_{bg} held at constant negative voltage to p-dope the nanotube sections outside the topgate region. The laser beam focus was adjusted to illuminate the whole gap in order to achieve maximum current signal.

Received 16 November 2007; accepted 22 February 2008; published 23 March 2008.

References

1. Saito, R., Dresselhaus, G. & Dresselhaus, M. S. *Physical Properties of Carbon Nanotubes* (Imperial College Press, London, 1998).
2. McEuen, P. L. & Park, J. Y. Electron transport in single-walled carbon nanotubes. *Mater. Res. Soc. Bull.* **29,** 272–275 (2004).
3. Park, J. Y. *et al.* Electron–phonon scattering in metallic single-walled carbon nanotubes. *Nano Lett.* **4,** 517–520 (2004).
4. Zhou, X. J., Park, J. Y., Huang, S. M., Liu, J. & McEuen, P. L. Band structure, phonon scattering, and the performance limit of single-walled carbon nanotube transistors. *Phys. Rev. Lett.* **95,** 146805 (2005).
5. Purewal, M. S. *et al.* Scaling of resistance and electron mean free path of single-walled carbon nanotubes. *Phys. Rev. Lett.* **98,** 186808 (2007).
6. Sazonova, V. *et al.* A tunable carbon nanotube electromechanical oscillator. *Nature* **431,** 284–287 (2004).
7. Appenzeller, J. & Frank, D. J. Frequency dependent characterization of transport properties in carbon nanotube transistors. *Appl. Phys. Lett.* **84,** 1771–1773 (2004).
8. Yu, Z. & Burke, P. J. Microwave transport in metallic single-walled carbon nanotubes. *Nano Lett.* **5,** 1403–1406 (2005).
9. Rosenblatt, S., Lin, H., Sazonova, V., Tiwari, S. & McEuen, P. L. Mixing at 50 GHz using a single-walled carbon nanotube transistor. *Appl. Phys. Lett.* **87,** 153111 (2005).
10. Plombon, J. J., O'Brien, K. P., Gstrein, F., Dubin, V. M. & Jiao, Y. High-frequency electrical properties of individual and bundled carbon nanotubes. *Appl. Phys. Lett.* **90,** 063106 (2007).
11. Zhang, M., Huo, X., Chan, P. C. H., Liang, Q. & Tang, Z. K. Radio-frequency characterization for the single-walled carbon nanotubes. *Appl. Phys. Lett.* **88,** 163109 (2006).
12. Karadi, C. *et al.* Dynamic-response of a quantum point-contact. *J. Opt. Soc. Am. B* **11,** 2566–2571 (1994).
13. Ferguson, B. & Zhang, X. C. Materials for terahertz science and technology. *Nature Mater.* **1,** 26–33 (2002).
14. Tonouchi, M. Cutting-edge terahertz technology. *Nature Photon.* **1,** 97–105 (2007).
15. Kohler, R. *et al.* Terahertz semiconductor-heterostructure laser. *Nature* **417,** 156–159 (2002).
16. Bockrath, M. *et al.* Luttinger-liquid behaviour in carbon nanotubes. *Nature* **397,** 598–601 (1999).
17. Yao, Z., Postma, H. W. C., Balents, L. & Dekker, C. Carbon nanotube intramolecular junctions. *Nature* **402,** 273–276 (1999).
18. Liang, W. *et al.* Fabry–Perot interference in a nanotube electron waveguide. *Nature* **411,** 665–669 (2001).
19. Kong, J. *et al.* Quantum interference and ballistic transmission in nanotube electron waveguides. *Phys. Rev. Lett.* **87,** 106801 (2001).
20. Peca, C. S., Balents, L. & Wiese, K. J. Fabry–Perot interference and spin filtering in carbon nanotubes. *Phys. Rev. B* **68,** 205423 (2003).
21. Burke, P. J. Luttinger liquid theory as a model of the gigahertz electrical properties of carbon nanotubes. *IEEE Trans Nanotech.* **1,** 129–144 (2002).
22. Yao, Z., Kane, C. L. & Dekker, C. High-field electrical transport in single-wall carbon nanotubes. *Phys. Rev. Lett.* **84,** 2941–2944 (2000).
23. Tombler, T. W. *et al.* Reversible electromechanical characteristics of carbon nanotubes under local-probe manipulation. *Nature* **405,** 769–772 (2000).

24. Minot, E. D. *et al*. Tuning carbon nanotube band gaps with strain. *Phys. Rev. Lett.* **90,** 156401 (2003).
25. Auston, D. H., Cheung, K. P. & Smith, P. R. Picosecond photoconducting Hertzian dipoles. *Appl. Phys. Lett.* **45,** 284–286 (1984).
26. Ketchen, M. B. *et al*. Generation of subpicosecond electrical pulses on coplanar transmission-lines. *Appl. Phys. Lett.* **48,** 751–753 (1986).
27. Ilani, S., Donev, L. A. K., Kindermann, M. & McEuen, P. L. Measurement of the quantum capacitance of interacting electrons in carbon nanotubes. *Nature Phys.* **2,** 687–691 (2006).
28. Geim, A. K. & Novoselov, K. S. The rise of graphene. *Nature Mater.* **6,** 183–191 (2007).
29. Lieber, C. M. & Wang, Z. L. Functional nanowires. *Mater. Res. Soc. Bull.* **32,** 99–108 (2007).

Acknowledgements

We thank J. Orenstein and L. Kouwenhoven for early assistance and discussions. This work was supported by the National Science Foundation (NSF) through the Cornell Center for Nanoscale Systems, and by the MARCO Focused Research Center on Materials, Structures, and Devices. Sample fabrication was performed at the Cornell Nano-Scale Science and Technology Facility (a member of the National Nanofabrication Infrastructure Network), funded by the NSF.
Correspondence and requests for materials should be addressed to P.L.M.
Supplementary information accompanies the paper on www.nature.com/naturenanotechnology.

Author contributions

Z.Z. and P.L.M. conceived the experiments. Z.Z. performed the experiments, and analysed the data together with N.M.G. and P.L.M. J.E.S. and A.L.G. provide valuable help on the optics. Z.Z. and P.L.M. co-wrote the paper. All authors discussed the results and commented on the manuscript.